Improvement of Wear Resistance of the Nickel Based Alloy Mixed with Rare Earth Elements by High Power Direct Diode Laser Cladding

Sayeed Mohammed[1] · Prabu Balu[2] · Arslan Ahmed[3] · Zhe Zhang[1] ·
Radovan Kovacevic[1]

Abstract

Wear is a restricting factor for steel in hostile environments but can be abated by laser cladding. Laser cladding of steel poses a promising solution to wear resistance. The high power direct diode laser is employed for the laser cladding of thicknesses of about 1.6 mm. Recently, the light rare earth metals have become important additions to smart materials, particularly Lanthanum oxide (La_2O_3) and Cerium Oxide (CeO_2), to improve microhardness and wear resistance. Layers of Ni-WC with 1% and 2% La_2O_3 and CeO_2 as alloying elements were cladded onto A36 steel substrate. The wear resistance and microstructure were studied with XRD and SEM. The hardness to modulus of elasticity ratio (H/E) was used to analyze the wear. It was found that the addition of 1% La_2O_3 or 1% CeO_2 to Nickel-based alloy (40% Ni-60% WC) improves the wear resistance.

Keywords Wear resistance · La_2O_3 and CeO_2 · Cladding · Steel

Introduction

The hardness and wear of steel limits its applications in extreme conditions. It was reported that the total cost of friction and wear globally was around US$285 billion in 2017, which was at some points more than the amount lost through corrosion of metals

✉ Radovan Kovacevic
  kovacevi@lyle.smu.edu

1   Research Center for Advanced Manufacturing, Department of Mechanical Engineering, Southern Methodist University, Dallas, TX 75205, USA

2   Coherent Inc., Santa Clara, CA 95051, USA

3   Center of Energy Science, Department of Mechanical Engineering, University of Malaya, Kuala Lumpur, Malaysia

[1, 2]. For example, the oil and gas industry uses deep-hole drilling tools which are constantly subjected to large forces and hostile conditions causing the deterioration of drilling tools by wear [3]. The thermal coatings were applied by chemical and physical vapor deposition, combustion flame spraying, arc wire spraying, high velocity combustion, and plasma spraying to prevent oxidation, wear, erosion, abrasion, and corrosion [4–6]. These techniques generated coatings with limited bond strength and not free from porosity. It was determined that the porosity, φ, adversely affect the modulus of elasticity, E, given by Eq. (1) [7].

$$E = E_i \left[\frac{(1-\varphi)^2}{1 + (2-3\upsilon_i)\varphi} \right] \tag{1}$$

where E_i and υ_i are the modulus of elasticity and Poisson's ratio of the material without porosity respectively.

With the extensive importance to cost, the laser is at the forefront of material processing. In 1960, Maiman discovered the first functional laser, but Gnanamuthu at Rockwell International Corporation first used laser for cladding in the 1970s [8, 9]. Cladding presents a new tribological solution to reduce friction and wear by boosting hardness with a significant enhancement in the service lifetime of the mechanical components [10, 11]. Popular lasers are fiber, CO_2, Nd:YAG, and the most recent one is high power direct diode laser (HPDDL). In HPDDL, the beam size and shape can be manipulated across the part. For example, to process large areas rapidly, the long axis of the beam can be oriented perpendicular to the scan direction. Kennedy et al. [12] reported that the diode laser also has more desirable modal stability than those of Nd:YAG or CO_2 lasers. Zhu et al. [13] further found that diode laser welding yielded reduced porosity as compared to that obtained by the CO_2 laser. Moreover, the HPDDL offers a high degree of control over clad width and thickness, and its high power results in metallurgically bonded clads with minimal part distortion [14]. Laser cladding can be designed to improve hardness and wear while keeping the toughness and strength of the base material [15].

In terms of engineering applications, the enhanced mechanical properties of Ni-WC alloys under high loads in unfavorable conditions makes them very attractive [16]. The reinforced particles added to Ni-based alloys further improve the wear and corrosion resistance of the coating [17]. It was determined that wear resistance of a given surface was improved by the deposition of the material of higher density and cohesive strength [18]. Coating with carbide particles embedded into a metal matrix with higher toughness and elasticity produces higher wear resistance.

The choice of alloys and the reinforced particles in the clad are vital for the wear resistance to a particular application. As compared to the other rare earth elements, La and Ce are of significant importance due to their large atomic radii (of 0.188 nm for La and 0.182 nm for Ce) and lower electronegativities (1.1 for La and 1.05 for Ce) enabling them to form positive ions (La^{3+} and Ce^{3+}) easily [19]. These ions react readily with other elements and affect their mechanical properties at high temperatures. It was determined that the addition of La and Ce increase the rate of reaction by lowering the activation energy in accordance with Arrhenius's equation of chemical reactions [20].

Amount of up to 1.0 wt.% of lanthana (or lanthanum oxide, La_2O_3) favors particulate dispersion homogeneity whereas more than 1.5 wt.% La_2O_3 impedes the activity of La_2O_3, resulting in a heterogeneous microstructure [21]. Ceria (or cerium oxide, CeO_2) is a reducible oxide agent and instrumental in corrosion protection [22]. The use of 0–8 wt.% of La_2O_3 and CeO_2 with Ni-based alloy has been studied for wear resistance and it has been reported that an amount more than 4 wt.% La_2O_3 or CeO_2 was detrimental for wear resistance [23, 24]. Amounts of La and Ce that were more than 1000 ppm caused inhomogeneity and increased grain size [20]. The hardness improved with 0.9 wt.% CeO_2, and porosity declined with 0.6 wt.% CeO_2 in Ni/WC coatings as opposed to Ni/WC coatings without CeO_2, indicating that the rare earth element content in the clad is important [25].

An extensive literature survey revealed a large number of studies on laser cladding of thickness under 0.1 mm, but not much research has been done on cladding of thickness to the order of 1.5 mm. The tools used in oil and gas industry are subjected to very large forces dictating the need for thicker coatings. Furthermore, there is limited data available on 1 or 2 wt.% addition of La_2O_3 and CeO_2 in Ni/WC clad. With this in mind, the authors of this study wish to research the wear resistance of thicker Ni/WC clad with 1 and 2 wt.% La_2O_3 and 1 and 2 wt.% CeO_2. In this study, 45 coupons were used to minimize deviations and improve repeatability.

Experimental Setup

Substrate and Clad Materials

Mild steel ASTM A36 plates of the dimensions 100 mm X 100 mm X 10 mm were used as the substrate. The powder of 38–39% Ni-60% WC was used along with 1–2% La_2O_3 or CeO_2 particles from 5 to 15 μm as alloying elements. The tungsten carbide powder was composed of crushed WC and W_2C particles of sizes ranging from 80 μm to 160 μm, and the grain size of Ni powder ranged from 1 μm to 80 μm. The powders were mixed in a Turbula shaker, which was operated in 3-D pulsing mode to blend the heavy particles of the powders.

Clad Fabrication

A HighLight D-series of high power direct-diode laser manufactured by Coherent Inc. was used in the experiment. The wavelength of the laser was 975 nm with a maximum power of 8 kW. The commercial laser head was seated on a 6-axis robotic arm manufactured by Kuka. The coupons were cleaned with sand blasting, which was followed by an acetone wash. The robotic arm and laser head were cleaned to prevent contamination. The cladding setup was composed of a high power direct diode laser, a powder feeder, a chiller for cooling the laser head, and nozzles to propel powder. The powder was carried by 7-channel symmetric co-axial nozzles along with argon gas at the focus of the laser beam. The argon was also used as shielding gas around the clad. The robot was positioned to produce a clad up to 30 mm in length. The laser beam was set at an angle of 10° to safeguard from back-reflection. A top-hat laser which had a uniform energy distribution with

a spot size of 12 mm × 1 mm was used in this experiment. The laser cladding setup is shown in Fig. 1.

Based on our previous studies, the clads formed with a scanning speed of 6.0 mm/s, a laser power of 2.6 kW, and a powder flow rate of 0.9 g/s produced a minimum number of cracks and porosity. Experimental plans were to combine 1% and 2% La_2O_3 with 39 wt.% Ni-60 wt.% WC and 38 wt.% Ni-60 wt.% WC, respectively, and 1% and 2% CeO_2 with 39 wt.% Ni-60 wt.% WC and 38 wt.% Ni-60 wt.%, respectively.

Wear Test

A high frequency reciprocating rig, Ducom TR-20EV-M3 ball-on-disc, was used in this study. The setup is shown in Fig. 2. The rig used a LVDT (Linear Variable Differential transducer) sensor, which is an electromechanical transducer. It converted the rectilinear motion into an electrical signal when coupled mechanically to an object. The ceramic (Al_2O_3, alumina oxide) ball of diameter 3.175 mm was used as a counter body to reciprocate on the clad. The ball had a stroke length of 2 mm and a reciprocating frequency of 5 Hz. The ball was loaded on the coupon with a normal force of 5 N. The tests were conducted in dry conditions at standard normal room temperature and pressure, and 50% relative humidity.

Results and Discussions

Microhardness

Microhardness is a material property which depends on intrinsic properties like crystal structure, cohesive energy, bond strength and extrinsic properties like lattice defects, size and distribution of grain, phase composition, and stress fields [26]. The
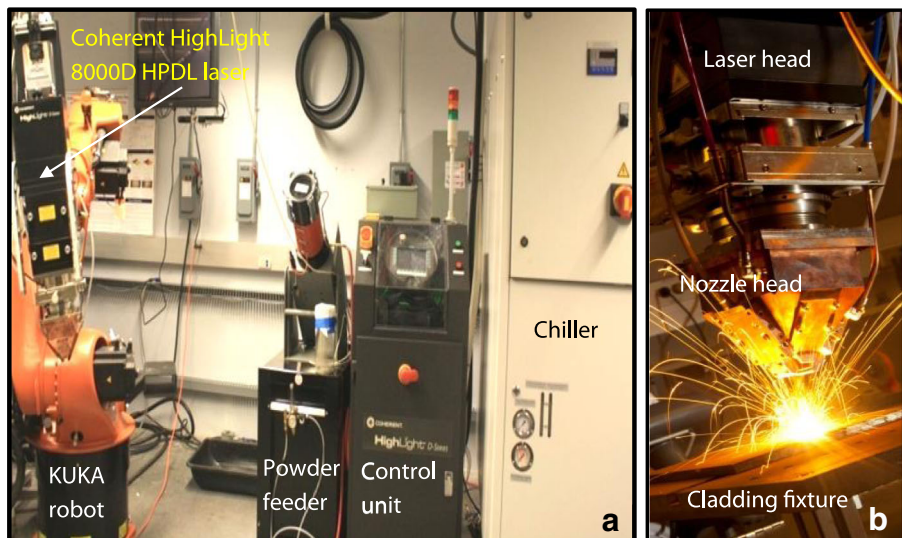

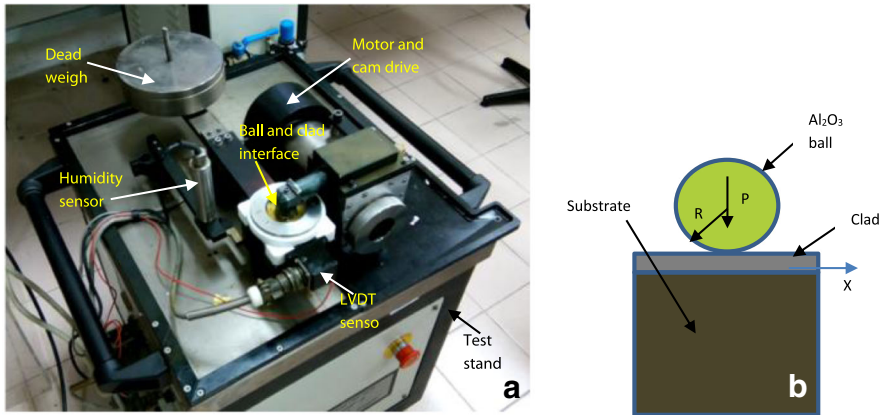Fig. 1 a Experimental setup for cladding. b Close-up of the laser and nozzle head

Fig. 2 **a** Wear testing machine. **b** Schematic of the alumina ball and clad surface

microhardness is estimated from the accumulated resistance of the chemical bonds to indentation and determined by the modulus of elasticity of the material from a macroscopic standpoint [27].

The substrate and clads of different alloying combinations were tested on the Clark Microhardness Tester (CM-700AT) for 15 s at 300 GF load, and the averages of Vickers microhardness values at eight locations across the clad for six combinations of coupons were recorded and plotted as shown in Fig. 3. The average microhardness of 40 wt.% Ni-60 wt.% WC increased to 551 HV as compared to 163 HV for the substrate. The addition of 1 wt.% La_2O_3 increased it to 580 HV and 568 HV for 2 wt.% La_2O_3. The clad with 1 wt.% CeO_2 had 572 HV and 560 HV for 2 wt.% CeO_2. It was reported that the increase in the microhardness by the addition of rare earth elements
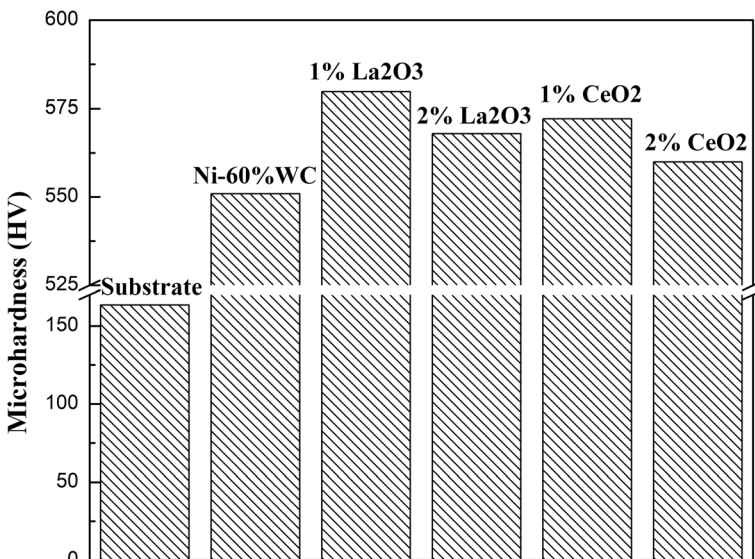

Fig. 3 Microhardness under different chemical compositions

was due to the improved bonding strength between Ni and WC particles and enhancement of WC distribution [28].

Wear Evaluation

Wear is defined as the removal of material from a body when subjected to contact and relative motion with another body. According to Archard's law, the wear volume loss is inversely proportional to the microhardness of the material [29]. In our work, using the depths of craters h, the wear volume loss V is calculated from Eq. (2) [30].

$$V = \frac{\pi h^2 (3r-h)}{3} \tag{2}$$

The wear volume loss was plotted in Fig. 4a and it was found to be the lowest for 1 wt.% La_2O_3–39 wt.% Ni-60 wt.% WC.

The specific wear rate is defined as the volume loss per unit normal force per unit sliding distance. The reciprocal of specific wear rate is known as wear resistance which is used in material selection for industrial applications. The wear resistances were computed and plotted in Fig. 4b. On average, the wear resistance for the cladded surface was found to be more than twice that of substrate. It was observed that 1 wt.% La_2O_3–39 wt.% Ni-60 wt.% WC clad had the highest wear resistance of those tested. While the addition of rare earth elements leads to only a marginal increase in the wear resistance, the significant increase in the corrosion resistance is notable and indicative of their utility [24].

Coefficient of Friction

The coefficient of friction, μ, versus sliding time, t, was plotted in Fig. 5 for the different combinations of clads. At the start, the increase in the coefficient of friction for all clads was due to high adhesive micro-contact between clad layer and counter body. As the wear test progressed till about 800 s, the contact area between the ball and the clad increased, resulting in a smaller normal pressure, and thus the μ value decreased. It was observed from the plot that the value of μ for the substrate was higher and had
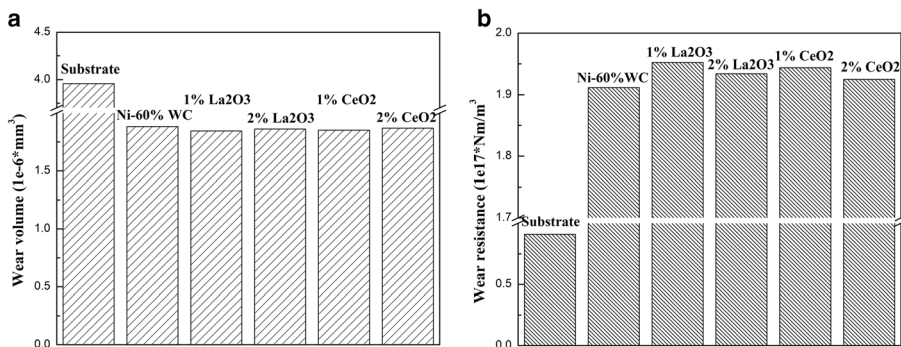

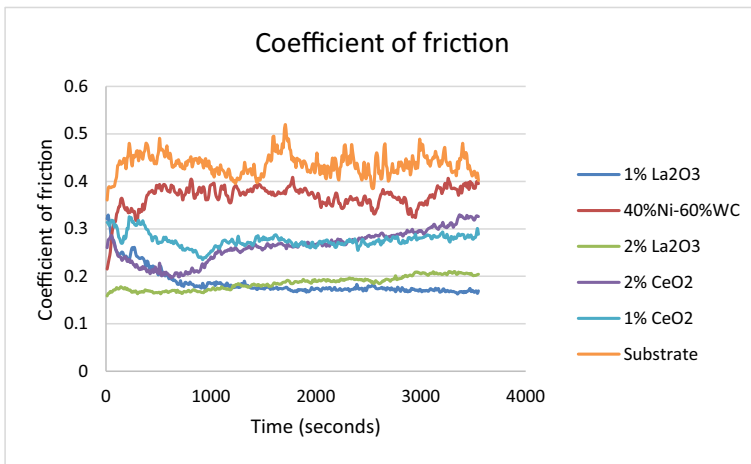Fig. 4 a Wear volume loss. b Wear resistance under different chemical compositions

Fig. 5 Coefficients of friction versus sliding time

larger fluctuations over time compared to the cladded surfaces. The higher fluctuations were explained by the "stick and slip" mechanism [31]. For the two surfaces in contact, the coefficient of friction increased as asperities entangled, and decreased with the rupture of junctions of the asperities. After 800 s, the slight increase in µ values can be attributed to the wear debris present at the interface of ball and clad surface. It was noticed that the values of µ were lower for clads as compared to substrate. This can be attributed to the higher microhardness of clads, which deterred the penetration and ploughing of asperities. The values of the wear resistance from the Fig. 4b and the corresponding coefficients of friction from the Fig. 5 indicated that lower the coefficient of friction, higher the adhesive wear resistance. It was noted that the 1 wt.% La$_2$O$_3$ clad had the lowest µ and minimum fluctuations during the wear.

H/E Ratio

Modulus of elasticity is a material property that describes the stiffness of a material and a harder material exhibits a higher value of modulus of elasticity. The elastic contact of a ball with the clad is shown in Fig. 6. Under the normal load N, the contact is no longer a point but enlarges into a crater, and the depth of the crater is expressed by Eq. (3)

$$h = \left(\frac{9N^2}{16E_o{}^2r} \right)^{1/3} \tag{3}$$

where r is radius of ball and E$_o$ is the overall contact modulus of elasticity of the ball and clad interface, or effective modulus [32].

The effective modulus is defined by Eq. (4) [32, 33].

$$1/E_o = \left(1-\upsilon_1{}^2\right)/E_{clad} + \left(1-\upsilon_2{}^2\right)/E_{Al2O3} \text{ or, } E_{clad} = \frac{1-\upsilon_1{}^2}{\left[\dfrac{1}{E_o} - \dfrac{1-\upsilon_2{}^2}{E_{Al2O3}} \right]} \tag{4}$$
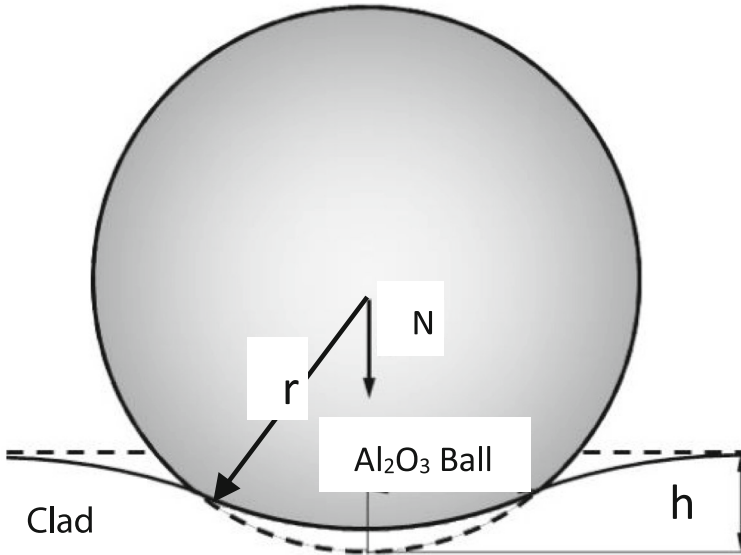
Fig. 6 Contact between Al_2O_3 ball and clad

Microhardness is not a direct measurement of wear because microhardness is a material property, and wear is a tribosystem property [34]. It was reported that H/E, related to elastic strain to failure, is a better parameter to predict wear rather than H or E alone [35]. The higher H/E ratio means a more durable coating with higher microhardness to resist plastic deformation relative to elastic modulus [36]. Using the values h from experiments of different combinations of clads, E_o-values were calculated from Eq. (3). The values of E_{clad} were evaluated from Eq. (4) with the Poisson ratios ν_1 and ν_2 as 0.24 and 0.21 for the clad and Al_2O_3 respectively, and $E_{Al2O3} = 350$ GPa. The values of E_{clad} for different combinations were presented in Fig. 7.

The elastic modulus of the substrate was found to be 197 GPa which is within 1.5% of the standard value of 200 GPa [27]. The elastic modulus value was improved by about three fold for 40 wt.% Ni-60 wt.% WC clad as compared to that of substrate. The value of H/E increased further by 3.5% for 1% La_2O_3–39 wt.% Ni-60 wt.% WC, and 2.3% for 2% La_2O_3–38 wt.% Ni-60 wt.% WC. The value of H/E increased slightly when 1% CeO_2 was added, and it remained almost the same when the amount was increased to 2% CeO_2.

The H/E ratios for different combinations were presented in Fig. 8. The values of H/E ratio were in agreement with the wear resistance values plotted in Fig. 4b, confirming the findings of previously reported studies [37, 38]. It was noticed that the value of H and E increased individually such that their ratio (H/E) also increased which validated the findings from Lima et al. [37]. The H/E ratio peaked for 1 wt.% La_2O_3–39 wt.% Ni-60 wt.% WC indicating its best wear resistance reaffirming the experimental results in Fig. 4b.
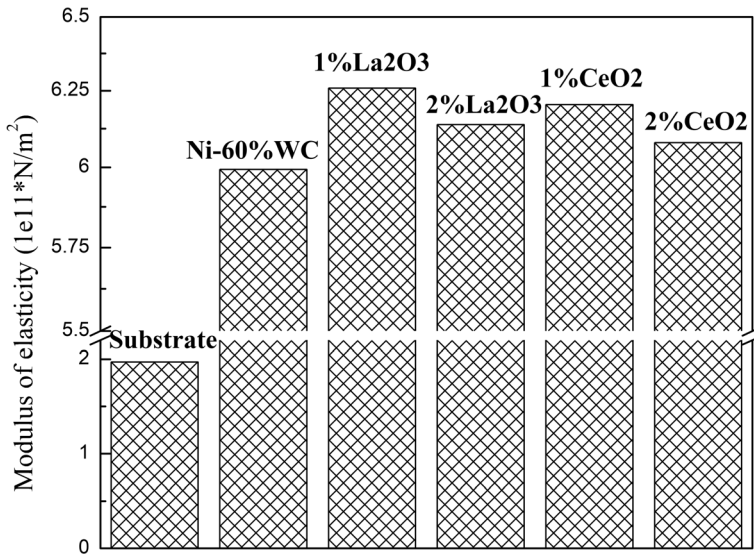
Fig. 7 Modulus of elasticity under different chemical compositions

Phases and Chemical Compositions

Rigaku II Ultima X-ray diffractrometer (XRD) was used in this analysis. XRD was performed in a 2θ range of 20-90°, functioning at 44 mA and 40 kV. A wavelength of
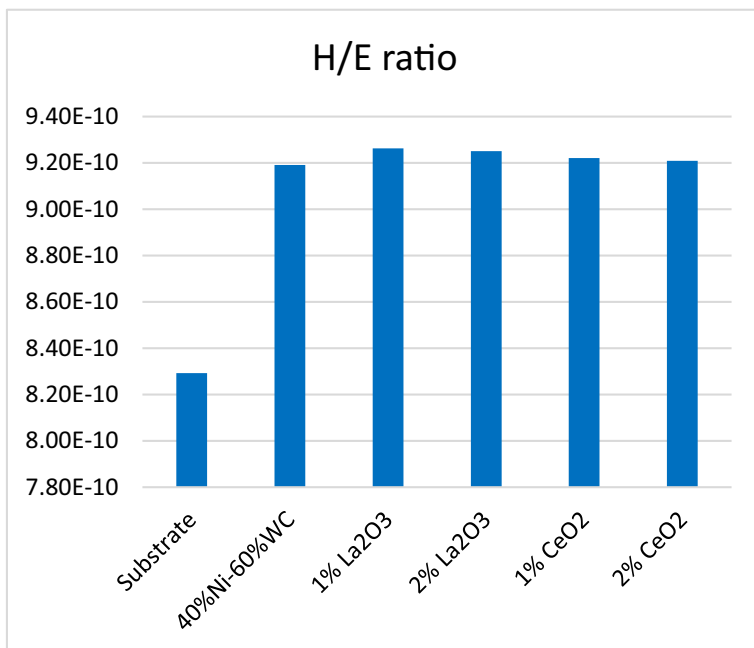

Fig. 8 H/E ratios under different chemical compositions

151.5 pm with radiations of Cu Kα and scan speed of 4 degree/min with a step size of 0.02º were employed in this experiment. Diffraction data was plotted, and the peaks in the plot were compared with the Joint Committee of Powder Diffraction Standards for phase identification.

The phases and chemical compositions of the different combinations were analyzed using XRD spectra and the ones for 1 wt.% La_2O_3–39 wt.% Ni-60 wt.% WC and 1 wt.% CeO_2–39 wt.% Ni-60 wt.% WC clads were presented in Figs. 9 and 10 respectively. The intensity, measured by the number of photons detected, was plotted against 2θ, the angle subtended between the incident and the diffracted ray. The crystal size, the orientation of crystals, and the texture determined the intensity of peaks and was represented as counts per second. The pointed peak for planes Ni(111), C(111) was observed due to the fact that iron and nickel crystallized in the face-centered cubic (FCC) system and have almost the same atomic size. In the XRD spectra, the other phases W_3C, W_2C, WC, Ni, and C were also detected. These complex phases are highly covalent carbide compounds and possess higher chemical stability and were formed because of the intense thermal power of the laser. The presence of complex structures and the networks of covalent bonds in these carbide phases culminated in increased wear resistance. Due to higher chemical activity of rare earth elements, rare-earth-transition intermetallics La_2NiO_2, $La_2Ni_5C_3$, and $Ce_2(WO_4)_3$ were observed as reported in the literature [23]. The addition of rare earth oxides led to the changes in intensities of the peaks. There were some peaks which could not be identified when compared to JCPDS and were hence not labeled. The smaller peaks after 90º were due to background noise.

Microstructure and Morphological Observations

A scanning electron microscope, 1450VPSE manufactured by Zeiss, was used to study the clad. The SEM consisted of secondary and back scattered electron detectors. The
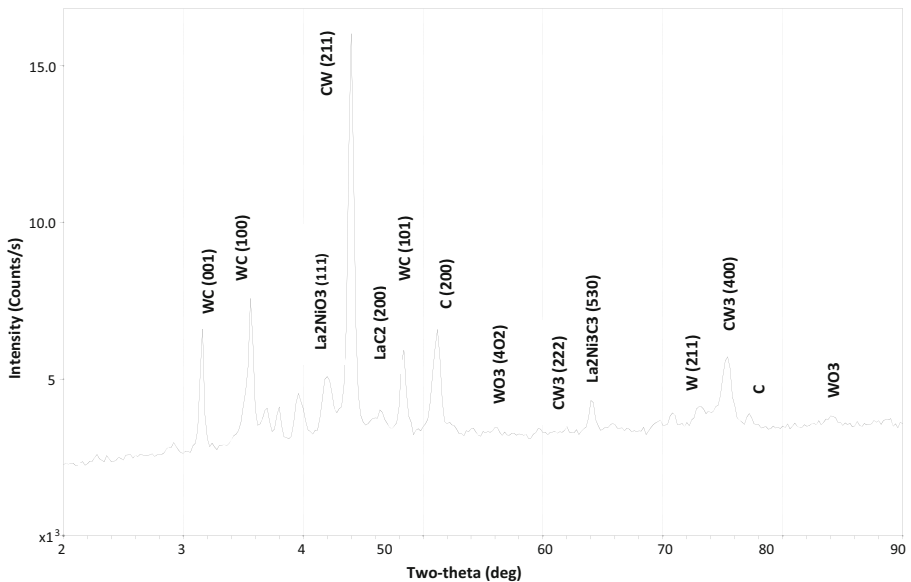

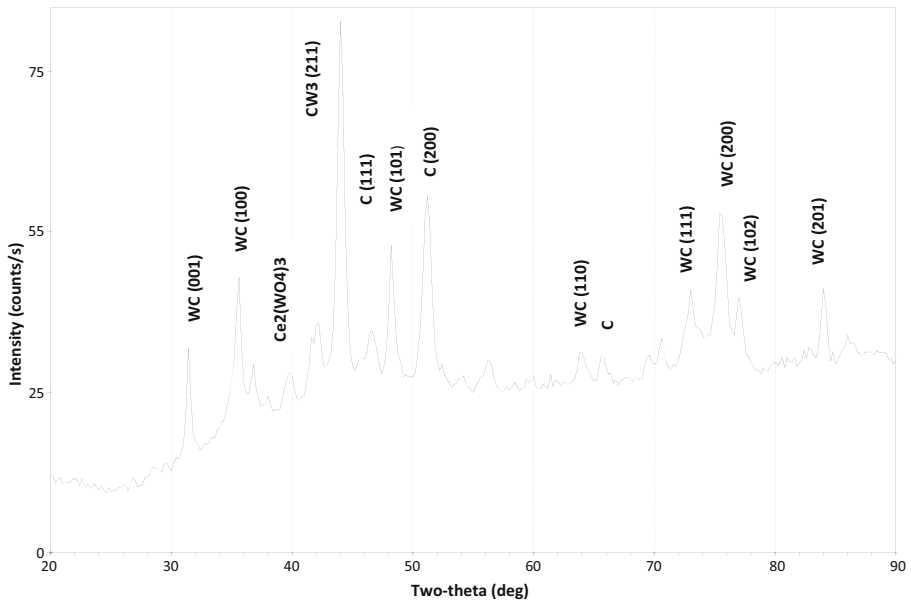**Fig. 9** XRD spectra of 1 wt.% La_2O_3–39 wt.% Ni-60 wt.% WC

Fig. 10 XRD spectra of 1 wt.% CeO$_2$–39 wt.% Ni-60 wt.% WC

cross-section micrographs at magnifications of 10X, 100X, and 500X were photographed. A visual inspection of the clad showed that the clad was free of cracks and well bonded to the substrate without delamination. The SEM examination of the clads revealed the thickness of clad to be approximately 1.6 mm (Fig. 11a). A distinct interface between clad and substrate demonstrated no dissolution. The WC particles of varying sizes and shapes were distributed in the Ni alloy matrix (Fig. 11b). The SEM micrograph showed prominent white WC particles with the precipitated carbides in the microstructure (Fig. 11c). There were no pin holes indicating no porosity. There were partially melted and broken particles of WC in the microstructure that can be ascribed to the significant difference between the thermal mismatch of the alloying particles. It was reported that the partial melting and thermal decomposition of WC results in the formation of W$_2$C [39].
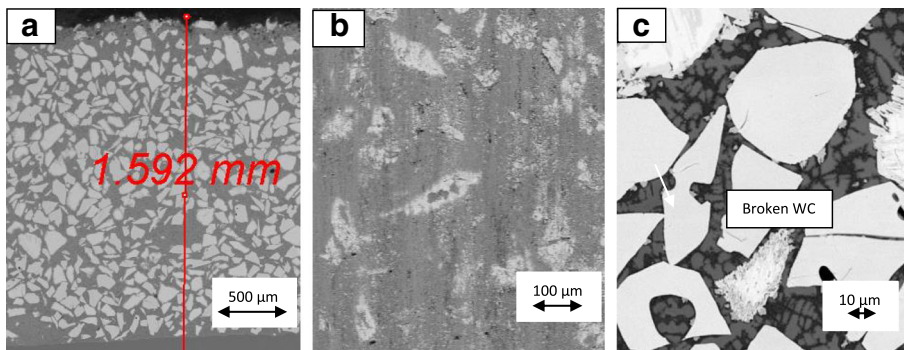

Fig. 11 Back scattered cross-sectional SEM micrographs of 40 wt.% Ni-60 wt.% WC clad layer **a** clad. **b** WC particles of different sizes. **c** broken particles of WC
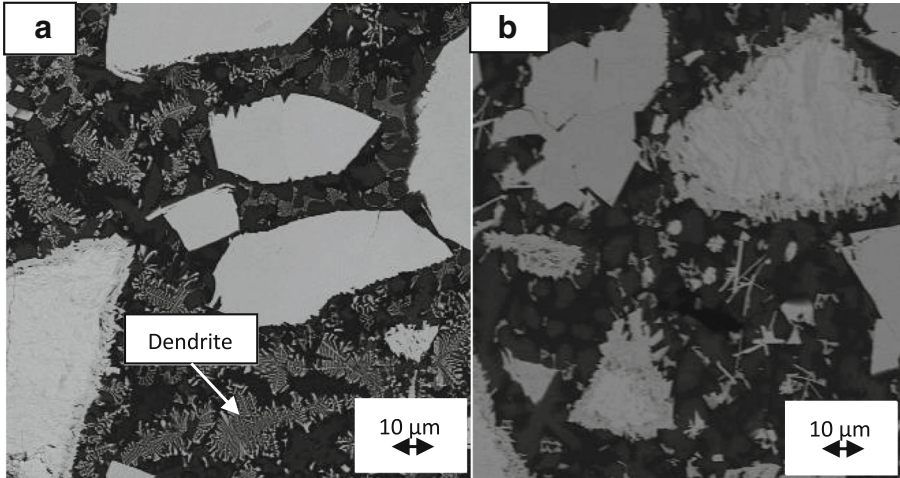
Fig. 12 **a** Back scattered electrons SEM micrographs of 1 wt.% La$_2$O$_3$–39 wt.% Ni-60 wt.% WC. **b** Back scattered electrons SEM micrographs of 1 wt.% CeO$_2$–39 wt.% Ni-60 wt.% WC

The greater covalent bond density and the associated three-dimensional network structures were responsible for the high microhardness of 40 wt.% Ni-60 wt.% WC clad as compared to the substrate. The WC particles were dissolved in the molten pool and the finer carbide particles were precipitated. The dispersion of finer particles improved microhardness in accordance with the Hall-Petch relation. The addition of rare earth oxides facilitated the formation of covalent bonds and microstructure refinement, producing a greater number of grain boundaries. The dislocation movement was arrested by the greater number of grain boundaries yielding higher microhardness [40]. Furthermore, they encouraged the production of carbide-enriched domains, facilitating higher microhardness contributing to higher wear resistance.

The morphology of clad layer with La$_2$O$_3$ or CeO$_2$ was shown in Figs. 12a, b. It was noticed that the addition of La$_2$O$_3$ or CeO$_2$ multiplied the number of crystal nuclei,
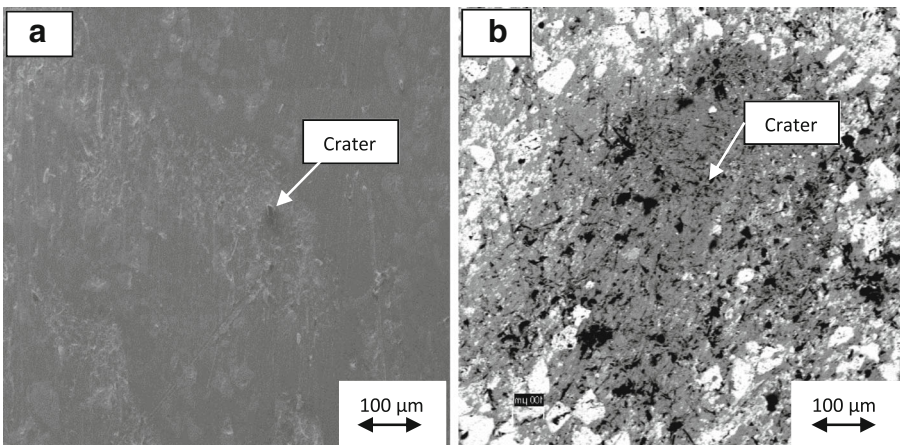

Fig. 13 **a** Secondary electrons detector SEM micrographs of 40 wt.% Ni-60 wt.% WC after wear test. **b** Back scattered electrons SEM micrographs of 40 wt.% Ni-60 wt.% after wear test
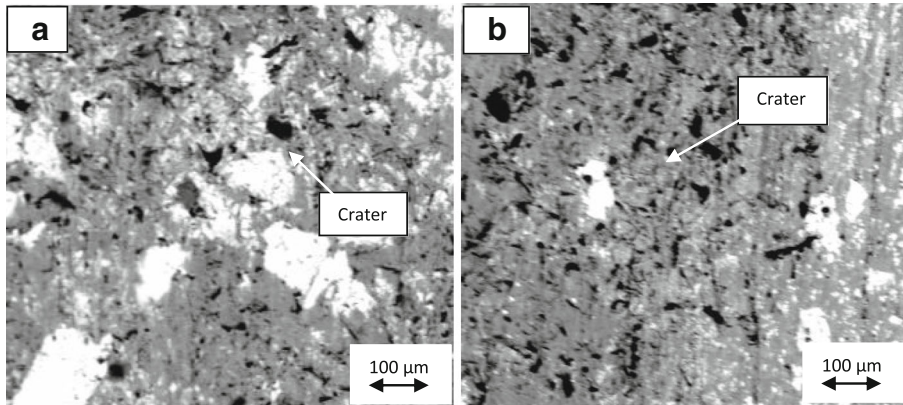
Fig. 14 **a** Back scattered electrons SEM micrographs of 1 wt.% La$_2$O$_3$–39 wt.% Ni-60 wt.% WC after wear test. **b** Back scattered electrons SEM micrographs of 2 wt.% La$_2$O$_3$–38 wt.% Ni-60 wt.% WC after wear test

facilitating the formation of a large number of grains. It was observed that the microstructure was transformed from coarse to fine grain, and a small number of snowflake structures were detected. Due to their large size, the rare earth oxides dispersed largely on the grain boundary, thereby impeding the grain growth [41]. Thus, a greater number of grains of smaller size were formed, enabling grain refinement. The improvement in wear resistance was due to the grain refinement by the addition of La$_2$O$_3$ or CeO$_2$ [42, 43]. In the SEM for La$_2$O$_3$, it was noticed that the spacing of the equiaxed dendritic arm was small (Fig. 12a) and for CeO$_2$, it was very small (Fig. 12b). The oxides of rare earth elements restrained the generation of columnar crystals and dendrites, which validated the findings of our preceding studies [43]. Thivillon et al. [44] reported that grain size decreased with higher nucleation rate. The finer grain led to higher dislocation density and the higher dislocation density led to the higher microhardness [45, 46].

It was inferred from Fig. 4a that wear volume loss depended on the alloying elements present in the clad layer. The smaller wear volume loss for 40 wt.% Ni-
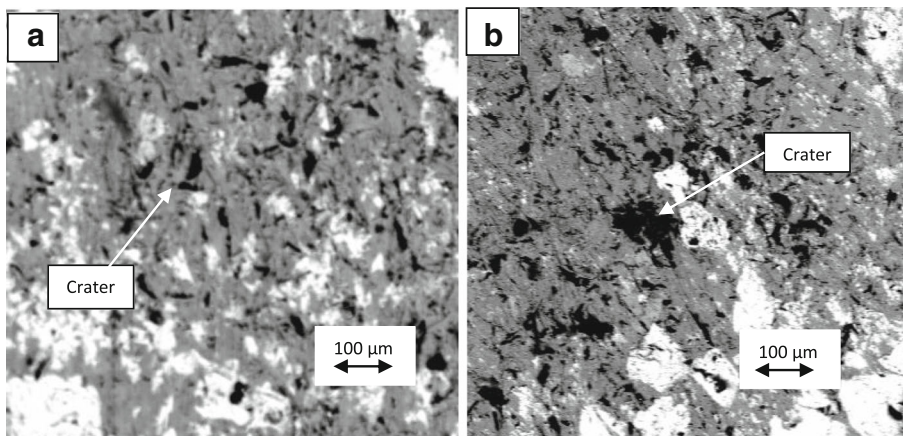

Fig. 15 **a** Back scattered electrons SEM micrographs of 1 wt.% CeO$_2$–39 wt.% Ni-60 wt.% WC after wear test. **b** Back scattered electrons SEM micrographs of 2 wt.% CeO$_2$–38 wt.% Ni-60 wt.% WC after wear test

60 wt.% WC as compared to that for substrate can be characterized by the nobler mechanical properties of hard phase WC. The wear volume loss was further reduced for clads with rare earth elements because of enrichment provided by rare-earth-transition intermetallics phases. The wear volume loss was the smallest for 1 wt.% La_2O_3 which can be attributed to a completely homogenized clad caused by the addition of 1 wt.% La_2O_3 [43]. The wear craters for different compositions were presented in Figs. 13, 14 and 15. It was observed that Fig. 14a had the most retained WC in the crater area after the wear test substantiating the experimental values in Fig. 3 and 4b indicating the highest microhardness and wear resistance respectively for 1 wt.% La_2O_3 clad.

Conclusions

This paper discussed the wear resistance of 40 wt.% Ni-60 wt.% WC clad when alloyed with 1 and 2 wt.% La_2O_3, and 1 and 2 wt.% CeO_2. The conclusions drawn from this research are as follows:

A uniform WC phase distribution was observed in the microstructure analysis of all clads. The rare characteristics of La_2O_3 and CeO_2 facilitated microstructure refinement. The clad adhered to the substrate with the smooth interface, inhibiting stress concentration at the interface. A planar solidification was detected at the interface of the substrate and the clad.

The microhardness of the cladded surfaces was found to be about three times of that of the substrate. The microhardness improved further with the addition of La_2O_3 or CeO_2. The coefficient of friction of the cladded surface relative to the substrate reduced by 16% for 40 wt.% Ni-60 wt.% WC, by 38% for 1–2 wt.% La_2O_3, and by 38% for 1–2 wt.% CeO_2. The percentage of reduction was almost the same for 1 and 2 wt.% La_2O_3 as well as 1 and 2% CeO_2.

The 40 wt.% Ni-60 wt.% WC clad improved the wear resistance of the substrate two-fold. The addition of La_2O_3 or CeO_2 increased the wear resistance further as compared to that of 40 wt.% Ni-60 wt.% WC clad. The addition of La_2O_3 increased the wear resistance slightly more than CeO_2 addition. The H/E ratio was the greatest for 1 wt.% La_2O_3, indicating that it had the strongest wear resistance of those tested.

It was observed that the amounts of 1 wt.% La_2O_3 and 1 wt.% CeO_2 were the most compelling for improving the wear resistance. As suggested by the literature, and confirmed by our results, the strongest expected effect of La_2O_3 and CeO_2 on wear resistance lies between 1% and 2 wt.%.

References

1. Holmberg, K., Erdemir, A.: Influence of tribology on global energy consumption, costs, and emissions. Friction. **5**(3), 263–284 (2017)
2. Oberle, T.L.: Properties influencing wear of metals. J Metals. **3**(6), 438–439 (1951)

3. Kembaiyan, K.T., Keshavan, K.: Combating severe fluid erosion and corrosion of drill bits using thermal spray coating. Wear. **186-187**, 487–492 (1995)

4. S. W. Huang, M. Samandia, M. Brandt. Abrasive wear performance and microstructure of laser clad WC/Ni layers. Wear (2004) 256 11–12 1095–1105

5. Rhys-Jones, T.N.: Thermally sprayed coating systems for surface protection and clearance control applications in aero engines. Surf Coat Technol. **43**(44), 402–415 (1990)

6. Hardwicke, C.U., Lau, Y.-C.: Advances in thermal spray coatings for gas turbines and energy generation: a review. ASM International. **22**(5), 564–576 (2013)

7. Ramakrishnan, N., Arunachalam, V.S.: Effective elastic moduli of porous ceramic materials. J. Am. Ceram. Soc. **76**(11), 2745–2752 (1993)

8. Maiman, T.H.: Stimulated optical radiation in ruby. Essentials of Lasers 134–136 (1969)

9. Gnanamuthu, D.S.: Laser surface treatment. Opt Eng. **19**(5), 783–792 (1980)

10. S.W. Huang, M. Samandia, M. Brandt. Abrasive wear performance and microstructure of laser clad WC/Ni layers. Wear (2004) 256 11–12 1095–1105

11. Chun Guo, Jianmin Chen, Jiansong Zhou. Effects of WC-Ni content on microstructure and wear resistance of laser cladding Ni-based alloys coating. Surf Coat Technol (2012) 206 8–9 2064–2071

12. Kennedy, E., Byrne, G., Collins, D.N.: A review of the use of high power diode lasers in surface hardening. J Mater Process Technol. **155-156**, 1855–1860 (2004)

13. Jinhong Zhu, Lin Li, Zhu Liu. CO_2 and diode laser welding of AZ31 magnesium alloy. Appl Surf Sci (2005) 247 1–4 300–306

14. Cui, C., Guo, Z., Liu, Y., Xie, Q., Wang, Z., Hu, J., Yao, Y.: Characteristics of cobalt-based alloy coating on tool steel prepared by powder feeding laser cladding. Opt Laser Technol. **39**(8), 1544–1550 (2007)

15. M. Laribi, A. B Vannes, D. Treheux. Study of mechanical behavior of molybdenum coating using sliding wear and impact test. Wear (2007) 262 11–12 1330–1336

16. Chang, J.H., Chou, J.M., Hsieh, R.I., Lee, J.L.: Corrosion behavior of vacuum induction-melted Ni-based alloy in sulphuric acid. Corros Sci. **52**(7), 2323–2330 (2010)

17. Qiwen, W., Mingxing, M., Cunyuan, P., Xiaohui, Y., Weiming, Z.: Corrosion resistance of laser produced in-situ particle reinforced Fe-matrix composite coating with high nickel content on spheroidal graphite cast iron. Phys Procedia. **41**, 276–281 (2013)

18. Lima, R.S., Marple, B.R.: Thermal spray coatings engineered fro nanostructured ceramic agglomerated powders for structural, thermal barrier and biomedical applications. J Therm Spray Technol. **16**(1), 40–63 (2007)

19. G. Balachandran. Extraction of Rare Earth for Advanced Application. Treatise on Process Metallurgy, Industrial Process (2014)

20. Ashassi-Sorkhabi, H., Moradi-Haghighi, M., Hosseini, M.G.: Effect of rare earth (Ce, La) compounds in the electroless bath on the plating rate, bath stability and microstructure of the nickel-phosphorous deposits. Surf Coat Technol. **202**(9), 1615–1620 (2008)

21. Go, D., Shen, Y.: The role of La_2O_3 in direct laser sintering of submicrometre WC-Co$_p$/cu MMCs. J Phys D Appl Phys. **41**, 1–11 (2008)

22. Stefanov, P., Atanasova, G., Stoychev, D., Marinova, T.: Electrochemical Deposition of CeO_2 on ZrO_2 and Al_2O_3 Thin Films Formed on Stainless Steel. Surf Coat Technol. **180-181**, 446–449 (2004)

23. K. L. Wang, Q. B. Zhang, M. L. Sun, X. G. Wei, Y. M. Zhu. Rare earth elements modification of laser-clad nickel-based alloy coatings. Appl Surf Sci (2001) 174 3–4 191–200

24. Wang, K.L., Zhang, Q.B., Sun, M.L., Wei, X.G., Zhu, Y.M.: Microstructure and corrosion resistance of laser clad coatings with rare earth elements. Corros Sci. **43**(2), 255–267 (2001)

25. Surajit Purkayastha, D. K. Dwivedi. Effect of CeO_2 on the Friction and Sliding Wear Performance of Ni/WC Coatings. International Conference on Advances in Electrical and Mechanical Engineering Phuket Thailand (2012) 18–19

26. de Carvalho Fernandes, S.M., Ramanathan, L.V.: Rare earth oxide coatings to decrease high temperature degradation of Chromia forming alloys. Mater Res. **7**(1), 135–139 (2004)

27. William F. Smith. Structure and Properties of Engineering Alloys. McGraw-Hill Book Company (1981)

28. Farahmand, P., Frosell, T., McGregor, M., Kovacevic, R.: Comparative study of the slurry erosion behavior of laser cladded Ni-WC coating modified by nanocrystalline WC and La_2O_3. Int J Adv Manuf Technol. **79**(9-12), 1607–1621 (2015)

29. Archard, J.F.: Elastic deformation and the laws of friction. Proceedings of the Royal Society of London. J Math Phys Sci. **243**(1233), 195–205 (1957)

30. Antunes, P.V., Ramalho, A., Carrilho, E.V.P.: Mechanical and wear behaviors of nano and microfilled polymeric composite: effect of filler fraction and size. Mater Des. **61**, 50–60 (2014)

31. F. P. Bowden, L. Leben. The nature of sliding and the analysis of friction. Proceedings of the royal society (1939) A 169 371–379
32. Negrea, A., Predoi, M.V.: The elastic contact of a sphere with an elastic half-space, a comparison between analytical and finite elements solutions. U P B Sci Bull. **74**(4), 69–78 (2012)
33. A. Z. Szeri. Fluid Film Lubrication; Theory and Design. Cambridge University press (1998)
34. Weng, F., Yu, H., Chen, C., Dai, J.: Microstuctures and Wear Properties of Laser Cladding Co-Based Composite Coatings on Ti-6Al-4V. Mater Des. **80**, 174–181 (2015)
35. Leyland, A., Matthews, A.: On the significance of the H/E ratio in wear control: a nanocomposite coating approach to optimized tribological behaviour. Wear. **246**(1-2), 1–11 (2000)
36. Benea, L., Basa, S.-B., Danaila, E., Caron, N., Raquet, O., Ponthiaux, P., Celis, J.-P.: Fretting and wear behaviors of Ni/nano-WC composite coatings in dry and wet conditions. Mater Des. **65**, 550–558 (2015)
37. Lima, M.M., Godoy, C., Modenesi, P.J., Avelar-Batista, J.C., Davidson, A.: A . Matthews. Coating fracture toughness determined by Vickers indentation: an important parameter in cavitation erosion resistance of WC-co thermally sprayed coatings. Surf Coat Technol. **177-178**, 489–496 (2004)
38. Rebholz, C., Leyland, A., Schneider, J.M., Voevodin, A.A., Matthews, A.: Structure, hardness and mechanical properties of magnetron-sputtered titanium-aluminum boride films. Surf Coat Technol. **120-121**, 412–417 (1999)
39. Wang, X., Zhang, M., Zou, Z., Qu, S.: Microstructure and Properties of Laser Clad TiC+NiCrBSi+Rare Earth Composite Coatings. Surface and Coatings Technology, vol. 161, pp. 195–199 (2002)
40. Yi, Y., Cho, P., Al Zaabi, A., Addad, Y., Jang, C.: Potentiodynamic polarization behavior of AISI type 316 stainless steel in NaCl solution. Corros Sci. **74**, 92–97 (2013)
41. Sharma, S.P., Dwivedi, D.K., Jain, P.K.: Effect of La_2O_3 addition on the microstructure, hardness and abrasive ear behavior of flame sprayed Ni based coatings. Wear. **267**(5-8), 853–859 (2009)
42. Jiang, X., Zhao, J., Jiang, X.: Correlation between hardness and elastic moduli of the covalent crystals. Comput Mater Sci. **50**(7), 2287–2290 (2011)
43. Farahmand, P., Liu, S., Zhang, Z., Kovacevic, R.: Laser cladding assisted by induction heating of Ni-WC composite enhanced by nano-WC and La_2O_3. Ceram Int. **40**(10), 15421–15438 (2014)
44. Thivillon, L., Bertrand, P., Laget, B., Smurov, I.: Potential of direct metal deposition technology for manufacturing thick functionally graded coatings and parts for reactors components. J Nucl Mater. **385**(2), 236–241 (2009)
45. Chu, J.P., Rigsbee, J.M., Banas, G., Elsayed-Ali, H.E.: Laser-shock processing effects on surface microstructure and mechanical properties of low carbon steel. Mater Sci Eng. **A260**, 260–268 (1999)
46. Lin, D., Ye, C., Liao, Y., Suslov, S., Liu, R., Cheng, G.J.: Mechanism of fatigue performance enhancement in a laser sintered superhard nanoparticles reinforced nanocomposite followed by laser shock peening. J Appl Phys. **113**(13), 133509 (2013)